Heat loads from ICRF and LH wave absorption in the SOL: characterization on JET and implications for the ITERLike Wall

L. Colas, Ph. Jacquet, M.L. Mayoral, G. Arnoux, V. Bobkov et al.

Citation: AIP Conf. Proc. **1406**, 183 (2011); doi: 10.1063/1.3664957
View online: http://dx.doi.org/10.1063/1.3664957
View Table of Contents: http://proceedings.aip.org/dbt/dbt.jsp?KEY=APCPCS&Volume=1406&Issue=1
Published by the American Institute of Physics.

Heat loads from ICRF and LH wave absorption in the SOL: characterization on JET and implications for the ITER-Like Wall

L. Colas[a], Ph. Jacquet[b], M.-L. Mayoral[b], G. Arnoux[a], V. Bobkov[c], M. Brix[b], M. Fursdon[b], M. Goniche[a], M. Graham[b], E. Lerche[d], J. Mailloux[b], I. Monakhov[b], C. Noble[b], J. Ongena[d], V. Petržilka[e], A. Sirinelli[b], V. Riccardo[b], Z. Vizvary[b], and JET-EFDA Contributors[*]

JET-EFDA, Culham Science Centre, OX14 3DB, Abingdon, UK
[a] CEA, IRFM, F-13108 Saint-Paul-Lez-Durance, France.
[b] Euratom/CCFE Association, Culham Science Centre, Abingdon, OX14 3DB, UK.
[c] Max-Planck-Institut für Plasmaphysik, EURATOM-Assoziation, Garching, Germany.
[d] Association EURATOM-Belgian State, ERM-KMS, Brussels, Belgium.
[e] Association EURATOM-IPP.CR, Za Slovankou 3, 182 21 Praha 8, Czech Republic.

Abstract. Heat loads from ICRF and LH wave absorption in the SOL are characterized on JET from the de-convolution of surface temperatures measured by infrared thermography. The spatial localization, quantitative estimates, parametric dependence and physical origin of the observed heat fluxes are documented. Implications of these observations are discussed for the operation of JET with an ITER-Like Wall, featuring Beryllium tiles with reduced power handling capability.

Keywords: ICRF, LH, JET, heat loads, plasma biasing, RF sheaths, Landau damping.

PACS: 52.55.Fa, 52.50.Qt, 52.35.Hr, 52.35.Mw, 52.40.Fd, 52.40.Hf, 52.40.Kh, 44.05.+e, 44.10.+i

Ion Cyclotron Resonance Frequency (ICRF) and Lower Hybrid (LH) systems are used in most of the JET experiments to provide heating and current drive and also for impurity and MHD control. However, parasitic LH and ICRF wave absorption in the plasma Scrape-Off Layer (SOL) can lead, for the ICRF case, to enhanced impurity release [1] and to enhanced heat fluxes on some Plasma Facing Components (PFCs) [2,3]. These heat loads were not an operational issue with the carbon wall. But from 2011 JET will operate with a new ITER-Like wall (ILW) [4] consisting mainly of Beryllium (Be) tiles in the main chamber and tungsten (or W-coated) tiles in the divertor, i.e. similar materials as envisaged for ITER. As the heat fluxes tolerated for Be tiles before melting are much lower than for Carbon Fibre Composite (CFC) tiles, experiments were carried-out in 2008-2009 to better characterize these wave absorption phenomena, and determine their driving parameters. The analysis relied on the de-convolution of surface temperature time traces from infrared thermography on three of the five ICRF antennas, the surrounding limiters and upper dump plates. The signal processing required a thermal modeling of the monitored PFCs, including

[*] See the Appendix of F. Romanelli et al., Proceedings of the 23rd IAEA Fusion Energy Conference 2010, Daejeon, Korea

Radio Frequency Power in Plasmas
AIP Conf. Proc. 1406, 183-190 (2011); doi: 10.1063/1.3664957

surface layers, which was subsequently assessed from the temperature measurements. Following this procedure, the paper investigates the heat fluxes corresponding to ICRF and LH power absorption in the JET SOL, as well as the thermal interplay between magnetically connected wave launchers. Implications of this analysis are discussed in the prospect of JET operation with the ILW. More detailed analysis is available in [5].

JET RF HEATING SYSTEM AND EXPERIMENTAL PROTOCOL

Figure 1 is an internal picture of JET by the time of the experiments, showing from left to right the LH Launcher, an ICRF A2-antenna and the ITER-Like ICRF Antenna (ILA). Each A2 antenna [6] is a toroidal array of four poloidal straps whose relative phase can be controlled, allowing launching waves with different spectra of wavevectors $k_{//}$ parallel to the magnetic field $\mathbf{B_0}$. Usually, dipole (phase difference π) or Current Drive (CD difference $\pm\pi/2$) phasings were used. Each antenna is covered in its plasma facing part with a Faraday screen consisting of tilted Be rods. It is surrounded by two poloidal limiters made of CFC and integrates in its middle a vertical CFC septum. The ILA [7] stacks on top of each other two 2(toroidal)×2(poloidal) strap arrays. Each array can be powered independently with toroidal dipole phasing. The ILA is surrounded by a frame of CFC tiles. The LH launcher [8] is a phased array of 32×12 waveguides arranged in 8×6 modules. The main parallel refractive index $n_{//}=k_{//}/k_o$ launched at 3.7GHz is adjustable in the range $1.4<n_{//}<2.3$ by controlling the phase between horizontally adjacent modules. The LH grill, plugged in a port, is mobile radially during pulses over several centimetres.

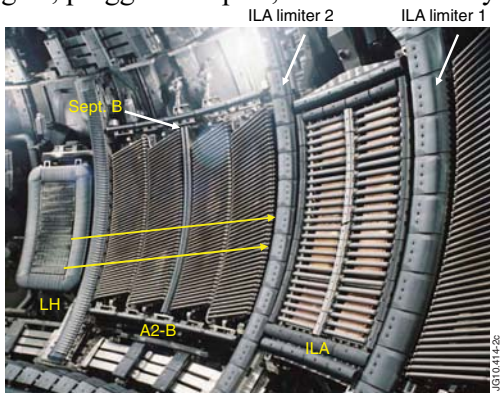

Figure 1. Photo of JET showing the LH launcher, A2 ICRF antenna B, and the ILA. Field line topology from the bottom rows of the LH launcher to ILA-limiter2 is also indicated.

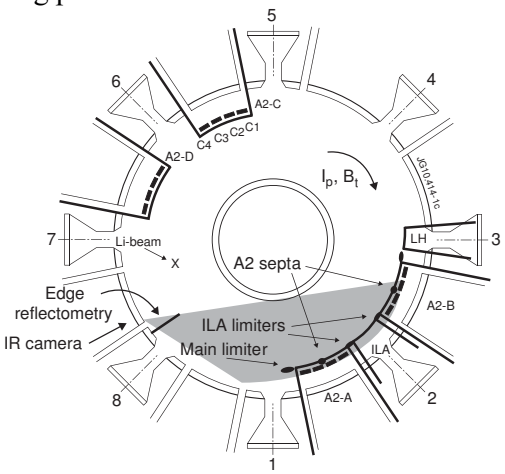

Figure 2. Top view of JET showing the five wave launchers and the IR camera view (in grey).

Figure 2 sketches the toroidal locations of the four A2 antennae, the ILA and the LH grill around the JET torus. The A2 antenna A, the ILA and half of the A2 antenna B can be observed by an infrared (IR) thermography diagnostic, whose viewing area is represented in grey. The IR camera [9] records the luminance in the range 3.97-4.00μm, with a time resolution of 16ms and an estimated space resolution of 3.5cm on the A2 septa. The IR luminance is translated into surface temperature, assuming gray-body radiation with an emissivity of 0.8 and spot size larger than the space resolution.

As on JET the heating pulse lengths are of the same order as the typical thermal time constants of the inertial PFCs, a linear de-convolution of dynamical temperature elevations $\Delta T_{IR}(t) \equiv T_{IR}(t) - T_{IR}(t_0)$ was necessary to estimate the applied heat fluxes $Q(t)$. Defining $F(t)$ as the thermal response of the analyzed PFC to a Heaviside excitation of unit amplitude applied from $t=0$, and assuming $Q(t)=0$ for $t<t_0$ one can show that [10]

$$\begin{bmatrix} T_{IR}(t_1)-T_{IR}(t_0) \\ T_{IR}(t_2)-T_{IR}(t_0) \\ \dots \\ T_{IR}(t_N)-T_{IR}(t_0) \end{bmatrix} = \begin{bmatrix} F(t_1-t_0) & 0 & \dots & 0 \\ F(t_2-t_0) & F(t_2-t_1) & \dots & 0 \\ \dots & \dots & \dots & \dots \\ F(t_N-t_0) & F(t_N-t_1) & \dots & F(t_N-t_{N-1}) \end{bmatrix} \begin{bmatrix} Q(t_1)-0 \\ Q(t_2)-Q(t_1) \\ \dots \\ Q(t_N)-Q(t_{N-1}) \end{bmatrix} \quad (1)$$

The thermal response $F(t)$ of the PFCs should be ideally measured in controlled conditions. Instead it was modelled using the ANSYS™ finite element software taking into account the 3D geometry of the tiles, as well as the anisotropic and temperature dependent properties of the CFC. The thermal model could subsequently be checked experimentally. Indeed, since we are mainly interested in peripheral RF power losses, $Q(t)=0$ can be expected after the heating phase. Alternatively the cooling of the PFC when the heating is switch-off is mainly determined by the shape of $F(t)$. The temperatures calculated from eq. (1) when forcing $Q(t)=0$ after the RF heating should therefore match the measured $T_{IR}(t)$. While the ANSYS thermal model was found satisfactory for de-convolution on the ILA limiter, it was necessary to add a ~1mm-thick layer of poorly conductive carbon-like material on top of the ideal model in order to reproduce the observed thermal decay on the A2 septa after heating by local power absorption. The presence of deposits was confirmed visually at shutdown [5]. Error minimization by a least square technique on the ΔT_{IR} decay was used to adjust the layer parameters on A2-A septum. Figure 3 illustrates the fit, showing how the associated change of $F(t)$ affected the magnitude of the estimated heat loads.

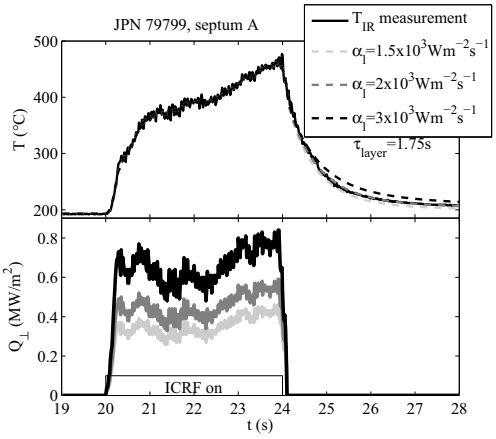

Figure 3. JPN 79799, measured $T_{IR}(t)$ on A2-A septum when antenna pair A+B is energized. Estimated heat flux $Q_{\perp}(t)$ normal to septum tile assuming time constant τ_{layer}=1.75s and three layer conductances α_l. Associated T decay computed for $Q_{\perp}=0$ imposed after heating pulse.

ICRF-RELATED HEAT LOADS AND ILA-A2 INTERACTION

Figure 4 is an IR picture taken along the camera view in figure 2, for a pulse in which 3MW of ICRF power was launched in L-mode from A2 antenna pair A+B. Hot spots light up along the A2 antenna septa as well as on their side limiters on the ILA frame. Rather than on the plasma-facing parts of these PFCs, the heat loads appear on their lateral sides, where field line incidence angle is non-grazing. In that case ΔT_{IR} reached up to 400°C on the hottest parts of A2 septum A after 3s of ICRF power application.

Figure 5 exhibits the thermal response of upper A2 septum B to several ICRF antenna combinations. The target plasma was in L mode with I_p=2 MA; B_T=2.7 T; Frequency: 42MHz; (H)D scenario with ~5%H. A2 antenna pairs A+B or C+D were energized at 2.8MW constant while the ILA power (upper or lower strap array) was stepped up gradually. While the conducted power onto the divertor tiles was checked to be independent of the RF launcher, Figure 5 shows that each antenna combination contributes differently to the local heat load on septum B. The C+D antenna pair is toroidally the farthest from the septum and is not connected magnetically. Upper and lower ILA are at the same toroidal location but only the upper ILA is magnetically connected to the area of interest and interacts more with this part of septum B. In contrast the upper and lower ILA produce similar heat fluxes in the upper part of septum A, where they can both be connected. It can be inferred that several physical processes are at play: a "global" one affecting the SOL uniformly (e.g. enhanced convected power) and a "local" effect in the magnetic shadow of the ICRF antennas.

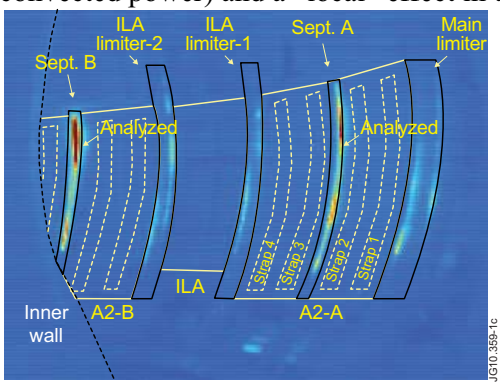

Figure 4. IR image, pulse 79799, t=23s. Superimposed are the A2 antennae A and half of B, the ILA, their poloidal limiters, and the A2 septa. The locations where surface temperature was analysed on figures 5 and 6 are also shown.

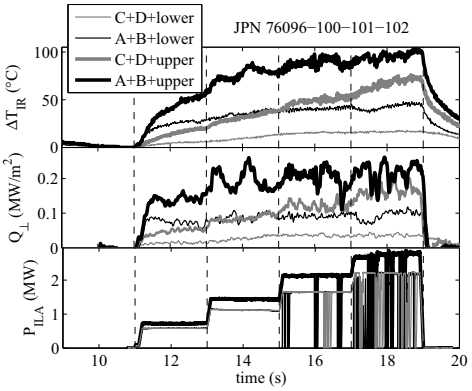

Figure 5. De-convolution of surface temperature on septum B during several combinations of A2 antenna pairs A+B / C+D and upper/lower ILA.

Figure 5 also evidences heat load oscillations at ~1Hz over time sequences at constant ICRF power. These oscillations, also visible on figure 3, are not an artefact of the de-convolution: $\Delta T_{IR}(t)$ decreases, which can only arise if $Q(t)$ is reduced. Part, but not all of these oscillations could be correlated with sawtooth crashes. Detailed analysis shows that the oscillations are not homogeneous vertically along septum B. The circumstances of their appearance and physical nature remain to be determined.

Figure 6 summarises the main parametric dependences of the "local effect", from ΔT_{IR} de-convolution on septum A (see Figure 4). In a series of L-mode discharges the following parameters were changed from pulse to pulse. 1°) Power balance between antennae A+B vs C+D. 2°) Antenna-separatrix distance and 3°) Strap phasing. Figure 6 shows that for prescribed phasing the heat-flux on septum tiles increases linearly with the local SOL density and with the RF voltage (averaged over the four straps) in the transmission lines feeding the antenna A. The SOL density was extracted from edge reflectometry profiles (measured not directly in front of the antenna, see figure 2), and was taken at the radial position of limiters at midplane. The scaling on figure 6 is consistent with simple models of power dissipation through RF sheaths rectification

[11], and with previous heat load studies on Tore-Supra [12] and JET [13]. In this formula $n_{e,lim}$ is indicative of the number of ions hitting the PFC while the ion energy gain across RF-enhanced sheaths scales like V_{RF}. CD strap phasing (more generally phasings producing low-$k_{//}$ spectra) leads to larger power dissipation than dipole (high-$k_{//}$ spectra). This observation is qualitatively consistent with reduced heating efficiency with low-$k_{//}$ phasings [13], as well as RF modelling showing enhanced line-integrated $E_{//RF}$ in these cases [14]. In these worst-case conditions the observed surface temperature of the septa was more than 800°C, and the estimated heat-flux normal to the tiles was up to 2MW/m^2. This corresponds to approximately 5MW/m^2 along flux tubes, when taking into account the angle of incidence of the field lines on the surface.

Assuming that an average of 1MW/m^2 is applied over the whole height of the septum (~1.5m) and a length of ~2cm along the tiles, the power lost on the septum is estimated to 30kW. Even when supposing that a similar amount of power is lost on three or four additional limiters or septa, this sums up only to a modest fraction of the transmitted 3MW ICRF power. Therefore the observed heat fluxes cannot explain quantitatively the the totality of heating efficiency reduction observed at low $k_{//}$ in [13]. One then needs to assume that in these cases most of the edge losses escape notice.

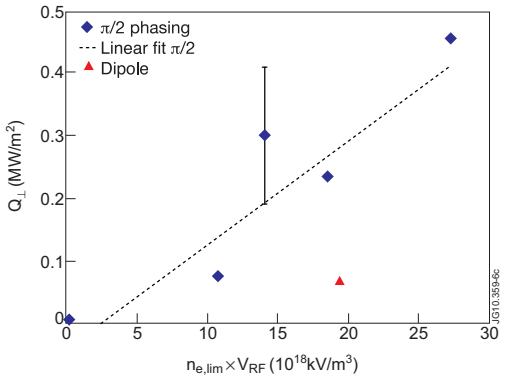

Figure 6. Estimated heat-flux on antenna A2-A septum versus the product of the SOL density and RF voltage, for two phasings. The error bar is representative of the flux oscillation during RF.

LH-INDUCED HEAT FLUXES AND INTERACTION WITH ICRF

The LH grill itself is not monitored by the thermography diagnostic, but it produces heat loads in view of the IR camera. They take the form of narrow spots at the extremities of flux tubes passing in front of the powered LH modules, with a poloidal extent of one LH waveguide height [15]. Some of them are visible on figure 7: depending on the plasma configuration and LH launcher radial position, LH hot spots can be observed on the septa of A2 antennae A or B (location 1 and 4), ILA poloidal limiters (2 and 3), main poloidal limiter (5), upper dump plates (6), inner (7) and outer divertor aprons (8), with sometimes connection lengths of few tens of meters. Hot spots are observed on the dump-plates (6) only for plasma configurations with a secondary X point at the top of the machine. In that heat fluxes are generally not seen in (7), and vice-versa. The characteristic spot shape is consistent with electron beams produced by Landau damping on high-$n_{//}$ spectral components of the LH near fields [16], either in co-current (locations 1-7) or counter-current direction (location 8).

Figure 8 shows an example of LH hot spot analysis. The plasma parameters in this pulse were: L-mode plasma; B_T=2.95 T; I_P=1.75 MA; q_{95}=5. D_2 gas injection close to the grill (~6×10^{21}e$^-$/s) was used to improve LH wave coupling. The LH grill, initially ~9 cm outside the separatrix, was retracted in 1cm steps at 8s and 10s. The LH fast electron beams generated from the four bottom rows of the grill were impinging on the

upper dump plates (location 6, figure 8b), and were intercepted by the ILA limiter (location 2-3) only for the most retracted position (10-12s). The output of T_{IR} de-convolution was translated into parallel heat fluxes $Q_{//}$ using reasonable assumptions on field line incidence angles. This yields $Q_{//}$~10MW/m^2 for both ILA limiter and upper dump plates. Figure 8 also illustrates that the heat flux on the dump plates does not importantly decrease when the launcher is retracted by 2cm during the pulse. This implies that the radial width of the LH wave absorption layer in front of the launcher is of 2cm or more [15]. This extension, combined with power density $Q_{//}$, allows evaluating the total amount of LH power deposited. For figure 8, assuming a beam radial width of 3.5cm, this represents 5% of the transmitted LH power. Assuming that comparable power is lost in the counter current direction, one can estimate that 10% of the launched LH power is absorbed in front of the grill in this case.

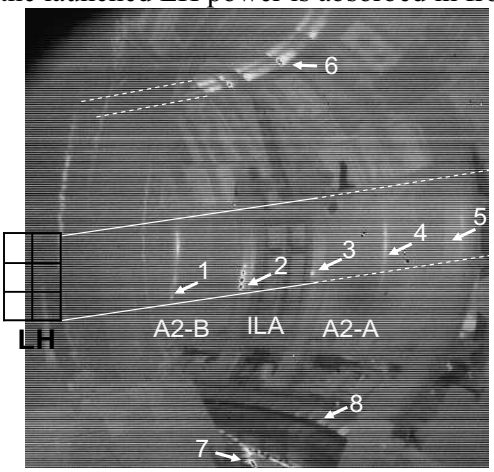

Figure 7. IR image showing LH hot spots during pulse 77393 t=12s. The approximate location of the LH launcher (not viewed by the camera) is shown. The launched LH power density is ~25MW/m^2, the top four and bottom four waveguide rows of the launcher were energized.

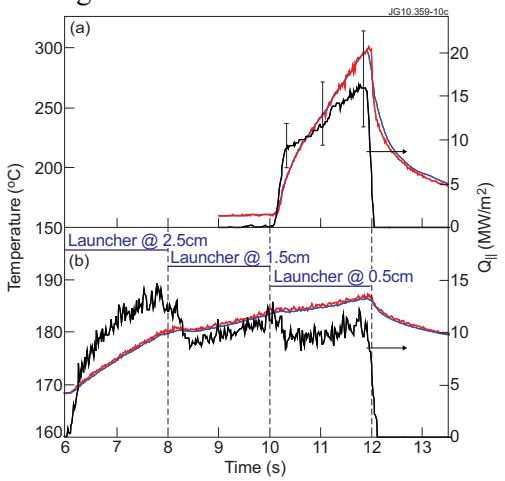

Figure 8. Pulse 77393. (a) Evaluation of peak heat flux along magnetic field-lines associated with the bottom hot spot on ILA limiter (location 2 on figure 7). (b) Heat flux along $\mathbf{B_0}$ evaluated from ΔT_{IR} de-convolution on the upper dump-plates, taking into account a flux expansion of 150 from plasma midplane toward the dump plates.

Figure 9 summarizes the main parametric dependences for the LH hot spots. The heat fluxes scale linearly with the LH power density ρ_{LH} and the local density $n_{e,launcher}$ at the grill mouth, as measured by a lithium beam connected magnetically from the top of the machine to the powered waveguide rows. By launching the same LH power P_{LH} with 20 or 28 waveguides along the same horizontal row, it was proved that ρ_{LH} was more relevant than P_{LH} in the scaling law. Li beam profiles also showed that the LH application was able to increase $n_{e,launcher}$, particularly in presence of local D_2 injection. This is attributed to neutrals ionisation by LH wave power in front of the grill [17].

Figure 10 shows the evolution of the 4 LH hot spots on the ILA limiters (locations 2-3 on figure 7) when both LH and the ILA, magnetically connected to the LH grill, were powered. Heat fluxes are modified by ICRF application, in different ways depending which hot spot, i.e. which magnetic field line is concerned. ICRF is known to modify the LH wave coupling by decreasing $n_{e,launcher}$ [18]. Similarly it is likely to modify the LH beam density, i.e. heat loads as the scaling on figure 9 involves

$n_{e,launcher}$ [19]. Figure 10 nevertheless suggests that the change is poloidally inhomogeneous and that $n_{e,launcher}$ could also locally increase during ICRF heating.

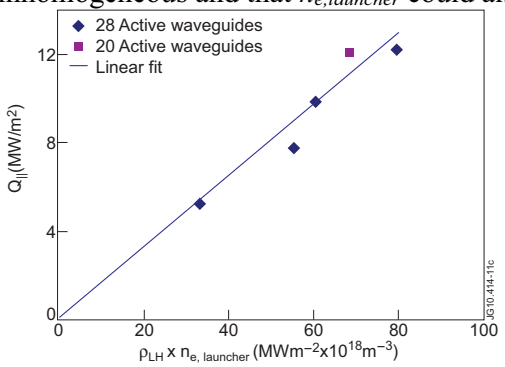

Figure 9. Estimated LH heat fluxes on dump plates, versus power density times local plasma density, for several sets of LH modules energized.

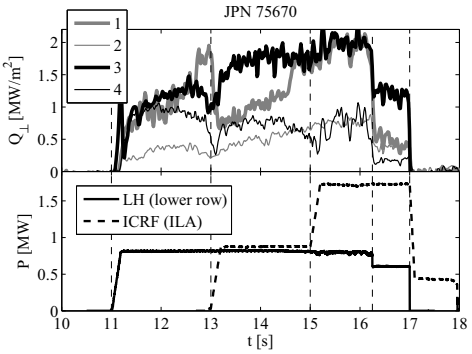

Figure 10. Estimated LH fluxes normal to ILA limiter during combined LH and ILA operation. Four hot spots are analysed, numbered 1-4 from bottom to top.

CONCLUSIONS AND OUTLOOK FOR ILW

ICRF and LH-related heat loads were characterized experimentally on JET using the de-convolution of surface temperature time traces from IR thermography. While relative variations are easy to evidence, absolute thermal flux quantification remains challenging in tokamak environment. Many uncertainties remain: calibration of the IR camera, under-resolution of the camera, assumed hot spot shape, unknown emissivity in the IR range, and uncertain surface thermal properties. Besides the computed heat fluxes were sometimes shown to oscillate over time sequences with steady plasma parameters. Although the ILW will add new measurement difficulties as Be is more reflective than present carbon tiles in the IR range, one can anticipate clean surfaces free of deposits at least after the restart. For these reasons it is important to confirm the estimated heat loads early during the ILW commissioning. To ensure ICRF and LH operation preserving the Be wall integrity, the viewing system is being extended. All A2 ICRF antennae will be monitored with visible cameras equipped with filters in the near IR range to detect temperatures above 750°C. The LH grill will be observed with a dedicated vertical IR camera. Protection against excessive surface temperatures will feature real time detection of hot spots and control of RF power.

Be tiles of the JET ILW have a power handling capability of 6MW/m^2-10s, assuming a cold start at 200°C. Regarding this constraint, the maximum heat flux estimated from past ICRF experiments (~2MW/m^2 projected onto tile surface) should not cause operational limits for typical JET pulse lengths (10s). The maximum measured LH heat flux of Q_0~7 MW/m^2 (very peaked, projected onto ILA limiter tiles) could be a concern for long pulses in worst-case conditions: ρ_{LH}>20MW/m^2, high density in front of the grill, large fraction of fast e$^-$ beam intercepted by limiter.

The spatial location of the heat loads, as well as their parametric dependence, were documented. They provide insight into the physical nature of the anomalous edge power losses and into ways to mitigate them. LH fast e$^-$ beams are a concern only if

they fall at large incidence onto outboard limiters, including the LH grill limiters (not observed so far). The spatial location of these hot spots can be controlled *via* the plasma configuration or the LH grill radial position. Although the ICRF-induced SOL modifications arise on the field lines exploring the vicinity of the powered launchers, their poloidal distribution along the septa as a function of strap phasing remains largely unknown. Their radial extension in front of the antennae is not known precisely, although it might affect possible interaction with the W-divertor.

Both the ICRF and LH local power absorption process (RF sheath rectification; e^- acceleration by high-$n_{//}$ spectral wave components) share parametric scalings involving the RF power, the wave spectrum and the local density near the launcher. At constant core density, the local density can be modified *via* the radial distance antenna/separatrix or *via* local gas injection. The formation of edge density profiles might also change with the ILW, whose recycling properties might be different from the previous JET vacuum chamber. An operational compromise needs to be found in order to improve the wave coupling while keeping surface temperatures acceptable.

Additional difficulties might arise when combining ICRF and LH waves. Firstly the optimal SOL conditions for one system might not be ideal for both. Secondly a complex ICRF-LH interplay was evidenced between magnetically connected wave launchers, with strong spatial variation and both hot spots enhancement and reduction. This could possibly complicate the LH heat load mitigation and the wave coupling. More detailed characterisation is necessary to define a global strategy.

Beyond the operational issues for the ILW, the experimental data grasped in 2008-2009 should be extended in the future campaigns in order to test physical models of peripheral wave-plasma interactions and be able to extrapolate their behavior to ITER.

Acknowledgements. This work, part-funded by the European Communities under the contracts of Association between EURATOM, CEA and CCFE and was carried out within the framework of the European Fusion Development Agreement. The views and opinions expressed herein do not necessarily reflect those of the European Commission. This work was also part-funded by the RCUK Energy Programme under grant EP/I501045.

REFERENCES

1. M. Bureš, et al., *Plasma Physics and Controlled Fusion* **33** No. 8 pp 937-967 (1991)
2. J. Mailloux, et al., *Journal of Nuclear Materials* **241-242** p745 (1997)
3. C.E. Thomas Jr, et al., *Journal of Nuclear Materials* **220-222** p531 (1995)
4. G. F. Matthews, et al., *Physica Scripta* **T138** 014030 (2009)
5. P. Jacquet & al "Heat-loads on JET PFCs from ICRF and LH wave absorption in the SOL", Submit. *Nuc. Fus.*
6. A. Kaye, et al., SOFE Conf. Proc., 16th IEEE/NPSS Symposium, Vol. **1** p736 (1995)
7. F. Durodie et al., *Fusion Engineering and Design* **74** (2005) 223-228
8. X. Litaudon and D. Moreau, *Nuclear Fusion* **30** (3), 471-484 (1990)
9. E. Gauthier, et al., *Fusion Engineering and Design* **82** 1335-1340 (2007)
10. J.-L. Gardarein, et al., *Fusion Engineering and Design* **83** pp 759-765 (2008)
11. F. W. Perkins, et al., Nuclear Fusion **29** No.4 pp.583-592 (1989)
12. L. Colas, et al., *Nuclear Fusion* **46**, pp. S500-S513 (2006)
13. E. Lerche, et al., in RF Power in Plasmas, AIP Conf. Proc. **1187**, pp 93-96 (2009)
14. V. Bobkov, et al., in RF Power in Plasmas, AIP Conf. Proc. **1187**, pp 125-132 (2009)
15. Ph. Jacquet, et al., in RF Power in Plasmas, AIP Conf. Proc. **1187**, pp 399-402 (2009)
16. V. Fuchs, et al., *Physics of Plasmas* **11** p. 4023 (1996)
17. M. Goniche, et al., *Plasma Phys. Control. Fusion* **51** (2009) 044002 (18pp)
18. K. Kirov et al. *Plasma Phys. Control. Fusion* **51** (2009) 044003
19. L. Colas et al., *Plasma Phys. Control. Fusion* **49** (2007) B35–B45